ORIGINAL ARTICLE

FFEMS Fatigue & Fracture of Engineering Materials & Structures   WILEY

Corrosion surface morphology-based methodology for fatigue assessment of offshore welded structures

Victor Okenyi[1] 🟢 | Shukri Afazov[1] | Neil Mansfield[1] |

Martin Alexander Eder[2] | Asger Bech Abrahamsen[2] | Søren Fæster[2] |

Christopher Gottlieb Klingaa[3] | Petros Siegkas[4] | Mahdi Bodaghi[1]

[1]Department of Engineering, School of Science and Technology, Nottingham Trent University, Nottingham, UK

[2]Department of Wind Energy, Technical University of Denmark, Roskilde, Denmark

[3]Danish Technological Institute, Aarhus C, Denmark

[4]Department of Mechanical Engineering and Materials Science and Engineering, Cyprus University of Technology, Limassol, Cyprus

Correspondence
Victor Okenyi, Department of Engineering, School of Science and Technology, Nottingham Trent University, Nottingham NG11 8NS, UK.
Email: victor.okenyi2020@my.ntu.ac.uk

Abstract

This work employed a novel corrosion-based fatigue model to determine the fatigue life of offshore welded structures to enable the fatigue assessment of welds under corrosive conditions. In addition to the material's ultimate strength, endurance limit, and stress ratio (mean stress effect), the model includes a corrosion factor concept to account for the impact of corrosion pits on the fatigue performance of welded S355 steel, which is the novel contribution in this paper. X-ray computed tomography scans of corroded S355 specimens in a salt spray chamber were characterized. Surface texture characterization was employed to obtain surface roughness, size, and aspect ratio of corrosion pits. The corrosion factor was determined based on notch and surface fatigue theories using the characterized pit size, aspect ratio, and surface roughness. Fatigue S-N curves were then predicted for critical pits and compared against the fatigue code DNVGL-RP-C203 and experimental data from the literature. The novel approach combining corrosion characterization method with corrosion-based fatigue model for the prediction of fatigue S-N curves provided a minor deviation of only 2.8% between predicted and measured data. This approach can potentially be integrated into predictive frameworks for the remaining life assessment of offshore structures.

KEYWORDS
corrosion characterization, corrosion pits, corrosion-based fatigue model, endurance limit, fatigue notch theory, fatigue surface theory, S355 S-N curves, stress concentration, surface roughness, X-ray computed tomography

Highlights

- Corrosion-fatigue challenges in wind turbine support structures has been addressed.
- Pit characterization has been conducted on a corroded steel coupon.
- Python code has been applied to obtain the surface roughness parameters of corroded steel.
- A corrosion-based model has been developed to predict fatigue strength.

1 | INTRODUCTION

Offshore wind energy generation can reduce the carbon footprint as there is a worldwide move towards installing more renewable energy capacity through offshore wind turbines (OWTs). Improving OWT structural performance can reduce costs associated with operation and maintenance. Structural performance must be closely researched with the global offshore wind energy expansion trend. In the United Kingdom, monopile supports (fixed-bottom OWT) are widely used due to installation convenience.[1] OWTs are subjected to cyclic loads from winds and waves. They operate in one of the harshest environmental conditions, making them vulnerable to fatigue damage accumulation. The wind energy market has seen continuous growth globally.[2] As the renewable energy sector grows, high-rated OWTs are deployed deeper into seawater,[3,4] where combined effects of cyclic mechanical loads and corrosion can create a detrimental effect. The design longevity and safety of OWTs, particularly their support structures, are crucial given their 20-year lifespan, considering that they can be in deep-sea subject to seawater corrosion. With many already nearing end-of-life OWTs, a comprehensive assessment of the fatigue life of offshore welded structural steel incorporating corrosion morphology effects is essential to reduce regular in-service inspections, ensure durability, and maintain operational efficiency. This justification underscores the need for thorough fatigue life analysis in offshore materials to ensure longevity and safety.

OWT monopiles are often constructed from welded hot-rolled structural steel plates, and their fatigue performance has been reported to be superior compared to normalized offshore steel.[5,6] Fatigue assessment factors such as defects caused by welding, oscillating stresses due to environmental loads, high stress concentrations at the intersection, and pits from corrosion due to seawater have been studied.[7–11] OWT monopiles are joined with V-shaped butt welds on both sides. The welding quality can significantly affect the fatigue performance of OWT monopiles as cyclic stresses at the welds can initiate fatigue cracks, particularly in the heat-affected zone (HAZ).[12] Manufacturing defects and residual stresses, stress concentration factor (SCF) at welds, surface roughness, and corrosion pitting at the surface are vital in the high cycle fatigue performance in offshore conditions. There is a need for all these fatigue-influencing factors to be holistically investigated to develop an improved way of assessing the fatigue life of offshore structures. The stress versus number of cycles (S-N) curve approach has been predominantly used to predict fatigue life,[13–15] and it has also been used in damage tolerant approaches.[16,17]

The fatigue capacity of structural steels in offshore applications is affected by various parameters, each of which can influence the quality and the mechanical properties. Although there are many reports on fatigue testing on structural steels, this review covers a representative number of studies[18–47] focusing on S355 butt-welded structural steels. These structural steels have been tested using a variety of test setups, loading conditions, welding types, and other postprocessing variables. The tested specimens have been subjected to various load-controlled fatigue conditions, including rotational bending, axial and bending fatigue testing at *stress* ratios of $R = -1$, 0, 0.1, 0.5 and different frequencies. The fatigue properties were affected by the surface roughness, the type of applied welding, the quality of the weldments, hardness, the thickness of the tested specimens, and the consideration of the environment (air or corrosive) for the fatigue tests. The predominant structural steel that has been taken into consideration is S355. In addition, the review has also considered other structural steels with the same range of yield strength and ultimate tensile strength (UTS).

The average UTS for S355 steel was found to be 546 MPa, whereas the average yield strength was 412 MPa. The fact that some of the reported hardness

values were within a specific range suggests that the testing was carried out from the base material to the weld zone, including the HAZ. The highest reported values were found to be at the weld region. For S355 steel grades, the elongation was in the range of 16.6%–36%. Metal active gas (MAG) welding and submerged arc welding (SAW) were the most common welding methods. Arc welding methods generally have been widely used in offshore structures, particularly in OWT.[48,49]

In addition to the reviewed literature,[18–47] S-N data from the design code standards BS7606,[50] DNVGL-RP-C203,[51] BS-EN1993-1-9,[52] and IIW recommendations[53] were also considered. The codes provided S-N curve values in both air and corrosive conditions in artificial seawater (ASW) and salt spray chambers (SSC). Welded specimens with one-side weld, usually of smaller thickness, appear to have better fatigue strength than two-side butt weld. In contrast, specimens without a weld have significantly superior fatigue life. This is consistent with the well-known fact that the weld zone generates a discontinuity in the material, and it is frequently sensitive to local stresses from which cracks typically initiate.[54] The high-frequency mechanical impact (HFMI) and shot peening (SP) treated specimens demonstrate that both post-weld treatment procedures enhance the fatigue life of structural steels. Identical specimens tested in SSC and ASW with the same stress ratio showed comparable fatigue performance in corrosive environments. However, compared to specimens tested in air, it was observed that corrosion negatively influenced the fatigue life of welded structural steel. Also, from the collected literature of fatigue tests in air and corrosive environments, it was observed that corrosion contributed to approximately 16% reduction in the fatigue strength of S355 structural steel.

The surface morphology of corroded offshore structures operating under seawater corrosion can be crucial. Pitting exists in the early life stages of marine structures, and it can be challenging to observe. Research showed that surface roughness of corroded carbon steel changed over time, and corrosion surface morphology can be quantified into shallow pits, overlapping pits and uniform corrosion stages.[55] Also, significant volumetric changes are observed over time, signifying the transition from pits to more uniform corrosion. Deep pits show higher stress concentrations, and the characteristics of corrosion pits or localized corrosion behavior can be fundamentally understood through skewness and kurtosis assessments.[56,57]

Statistical analysis of the probability distributions have been employed as a valuable tool in understanding corrosion pits, which also involved time. This research establishes a connection between the pit characterization, the localized stresses, and its relationship to cyclic loading under corrosive conditions. The pragmatic use of the S-N curve concept to encapsulate the correlation between corrosion defects and fatigue life, particularly in welded components used in offshore structures, needs to be more rigorously researched. The primary obstacles stem from the difficulty in determining the pit size, position, form, location and how they interact with fatigue strength and loading cycles. A predictive model based on the endurance limit approach has been used to determine surface factors and defect factors in metal additive manufacturing.[58] Still, the research work did not include any consideration of corrosion or welding. Despite the conducted research in the literature, the relationship between corroded surface morphology and fatigue life can be improved, especially in welded parts used in offshore structures. One of the challenges in fatigue assessment in corrosive environments is constructing a S-N curve that factors the surface morphology, including pit size and surface roughness. To address this challenge, a novel corrosion surface morphology-based fatigue methodology is proposed to predict the fatigue performance (S-N curve) of offshore welded S355 structural steel for the first time.

The research methods and the corrosion surface morphology-based methodology are first presented, followed by results and discussion. The paper includes characterization of precorroded specimens from a salt-spray chamber and artificial seawater, identification of critical pits, development of a fatigue model considering pit size and aspect ratio as well as surface roughness effects using statistical analysis of the probability distribution of variable depth, prediction of S-N curves and comparison with data from fatigue codes and literature.

2 | RESEARCH METHODS

2.1 | Corroded specimen

An investigation was conducted to determine the corrosion characterization of precorroded welded S355J2 + N steel specimens. Corrosion observed in a realistic offshore environment was replicated in lab-scale dog-bone welded specimens. Although corrosion is a time-dependent phenomenon, this research focused on the influence of corrosion environments as specimens were corroded in SCC and ASW conditions in compliance with standards.[59] Figure 1 shows the corrosion effects on a welded sample where the excess material of the weld was machined before corrosion.

2.2 │ X-ray computed tomography of specimens

The S355J2 + N sample was scanned using X-ray computed tomography to characterize the precorroded surface. The scans were carried out using the Zeiss Xradia 520 Versa with an X-ray energy of 160 keV, an exposure time of 13 s where 3601 projections were acquired, covering a 360° rotation of each sample, on a 2k × 2k pixel size charge-coupled device (CCD) detector. The scans were reconstructed using the Feldkamp, Davis, and Kress filtered back projection algorithm[60] to 2k × 2k × 2k volumes with a voxel size of 12.63 μm. Once the scanning process was concluded, the 3D renderings were obtained by setting a constant threshold in the reconstructed volumes and presented in Figure 2A–C. This model offered in-depth insights into the structure of the specimen and the defects brought on by corrosion. This study has considered the heat-affected zone (HAZ) to access the most critical fatigue regions for crack origination reported for welds.[9,42,43,53]

The method applied in the corrosion characterization involved the use of the commercially available Avizo 3D software[61] to visualize the corroded surfaces. The visualization is based on segmentation conducted with a threshold masking value of 47,000, which was used across all scans for consistency. Three-dimensional surfaces were generated with no smoothening to provide an actual surface view, as illustrated in Figure 2D.

2.3 │ Corrosion pit characterization approach

Subsequently, the GOM Inspect software[62] received the precorroded 3D surface, which was aligned to the uncorroded 3D geometry using the uncorroded edges as reference points. A surface deviation map was calculated after the alignment. A pit depth (a) was determined by the value of the surface deviation, while a pit diameter (D) at the surface was characterized by a circular shape. This
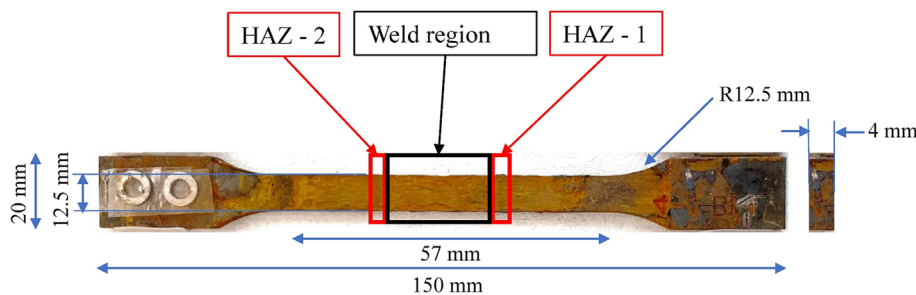

FIGURE 1 Precorroded S355J2 + N structural steel specimen. [Colour figure can be viewed at wileyonlinelibrary.com]
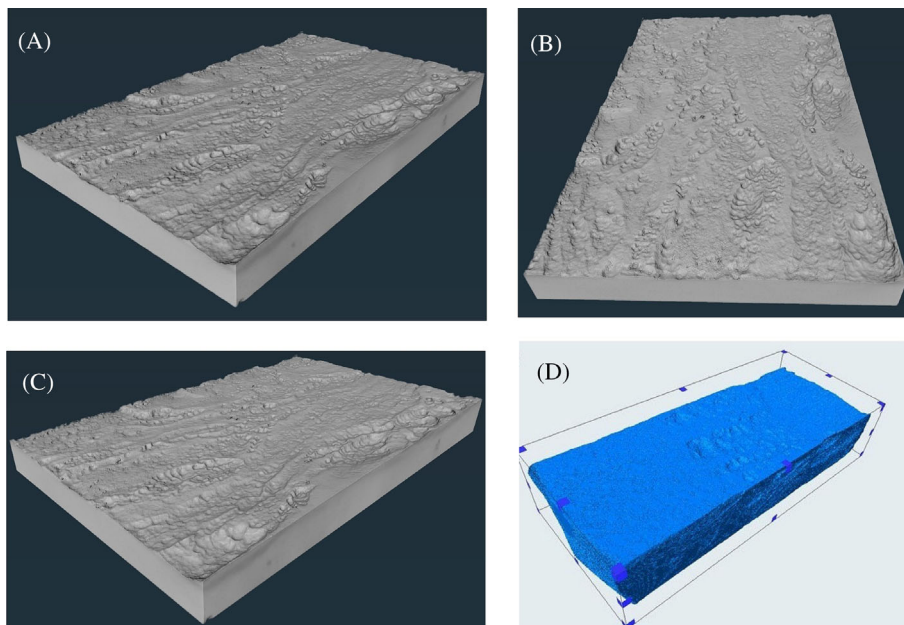

FIGURE 2 (A–C) Corroded specimens obtained from 3D CT scanning of a corroded sample: (D) segmented surface in Avizo using X-ray computed tomography data. [Colour figure can be viewed at wileyonlinelibrary.com]

characterization method was applied to several critical pits with great aspect ratio (a/D).

2.4 | Method for obtaining surface roughness

An examination of the surface roughness was performed on the corroded specimens using a tool written in Python[63] that was developed by Klingaa et al.[64] The applied method was a fitted-ellipse method based on a fitted geometry approach, which allowed for both qualitative characterization and quantitative analysis of the corroded specimen's surface. However, this method's effectiveness was contingent on the quality of the CT scans, which is a possible constraint, but high-quality scans were taken in this study. This approach proved to be highly efficient for the purpose at hand. It starts with manually feeding an image stack into the computer program ImageJ,[65] followed by execution of the Python code.[63] After determining the threshold value in ImageJ, it was incorporated as an input in the Python code, automating the rest of the image analysis and computational process. The Python code generated 3D scatter plots, leveraging the vertices of meshed surfaces to visualize both the CT-scanned surface and the fitted elliptical surface.

The initial step consisted of importing 1178 image stacks into the ImageJ[65] to establish a segmentation threshold for the image stack. The image stacks were divided into two distinct groups: steel substance and air. The Renyi Entropy function approach within ImageJ was employed to improve the segmentation of grayscale images into features of interest and background. After that, the image stacks were imported into the Python code, and the analysis results were based on the determined segmentation thresholds. After that, the standard ISO 25178-2:2021[66] was applied to generate surface texture parameters.

2.5 | Corrosion-based fatigue methodology

A corrosion surface morphology-based methodology is presented in Figure 3 to assess the fatigue life of offshore welded steel exposed to corrosion in seawater. The methodology consists of corrosion characterization, fatigue modeling and prediction of S-N curve. The corrosion characterization consists of identifying the pit size, pit shape (aspect ratio) and surface roughness at the pit. The information from the characterization (size, aspect ratio and surface roughness) is then used as an input into a fatigue model based on the endurance limit approach.[58] The pit size and aspect ratio were modeled using a notch theory by identifying the notch sensitivity of the material. The surface roughness generated from corrosion is also included in the fatigue model using a surface theory. The detail of incorporating the corrosion factor into the Basquin equation is provided. The capability of the fatigue model is to predict S-N curves for a given input from the corrosion characterization.

2.6 | Corrosion-based fatigue model with incorporated corrosion factor

In this section, a corrosion-based fatigue model is developed and presented. The impact of corrosion at the surface is crucial to the material's fatigue strength. In industry, the endurance limit approach is widely used. The approach consists of approximating the stress amplitude at 10^6 cycles and 10^3 cycles, assuming a stress ratio of $R = -1$. Equation (1) shows that at 10^3 cycles, the fatigue stress amplitude is 90% of the UTS, while at 10^6 cycles (see Equation 2), the fatigue stress amplitude is approximately 50% of the UTS. The values of 0.9 and 0.5 (endurance limits) are derived from empirical observations and experimental data for many materials, especially ferrous alloys.[67] Thus, they are given by

$$\sigma_a^f\left(N = 10^3\right) = 0.9 \times \sigma_u \text{ at } 10^3 \text{ cycles} \tag{1}$$

$$\sigma_a^f\left(N = 10^6\right) = 0.5 \times \sigma_u \text{ at } 10^6 \text{ cycles} \tag{2}$$

where σ_a^f is the fatigue stress amplitude, N is the number of cycles, and σ_u is the UTS.

The mean stress effects, σ_m, using the Goodman approach is introduced together with a newly defined corrosion factor, f_c, into Equation (2) to obtain Equation (3).

$$\sigma_a^f = 0.5 f_c \sigma_u \left(1 - \frac{\sigma_m}{\sigma_u}\right) \text{ at } 10^6 \text{ cycles} \tag{3}$$

The influence of the pit morphology and the surface roughness determines the corrosion factor. Considering the corrosion factor and the mean stress effect represented by the stress ratio R, the model is now expressed in terms of a stress range, σ_r^f, similarly obtained in[58]

$$\sigma_r^f = 1.8\sigma_u \text{ at } 10^3 \text{ cycles} \tag{4}$$
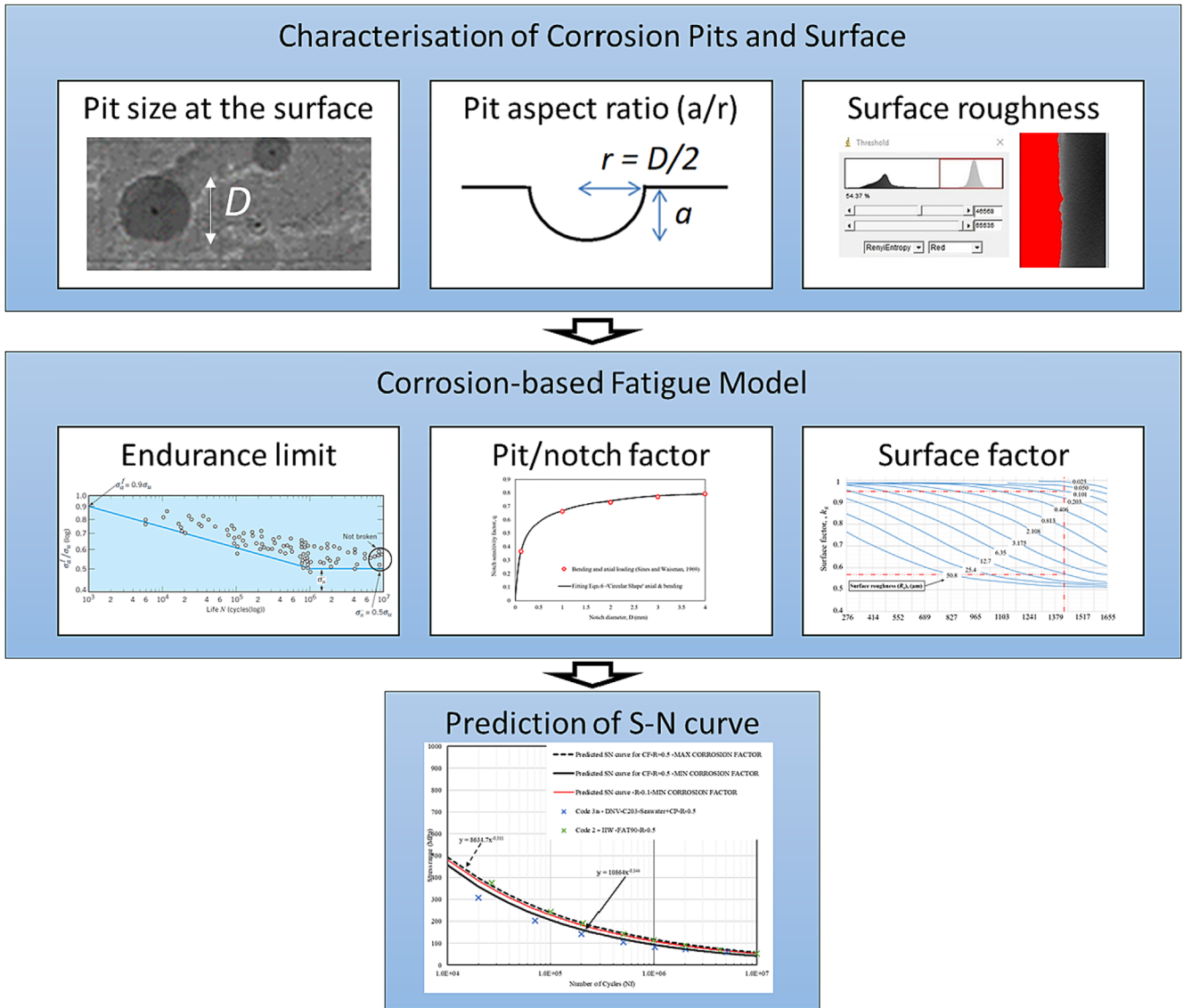
FIGURE 3 An overview of the corrosion-based fatigue methodology. [Colour figure can be viewed at wileyonlinelibrary.com]

$$\sigma_r^f = \frac{\sigma_u f_c}{1 + 0.5 f_c \left(\frac{1+R}{1-R}\right)} \text{ at } 10^6 \text{ cycles} \quad (5)$$

$$\sigma_r^f = A N_f^{\,n} \quad (6)$$

Equation (5) shows that the fatigue stress range depends on the UTS, stress ratio R (mean stress effect) and the newly introduced corrosion factor, which further reduces the endurance limit. Equations (4) and (5) were utilized to produce two points corresponding to the S-N curves at 10^3 and 10^6 cycles, respectively. After that, the two generated data points were fitted into the Basquin fatigue formula (Equation 6) to derive the material fitting constants, which are denoted by A and n.

The corrosion factor, f_c, represents the shape of the pit (size and aspect ratio) and the surface roughness at the pit. To represent this, the corrosion factor is expressed as a product of a notch factor, f_n, and a surface factor, f_s, by

$$f_c = f_n f_s \quad (7)$$

The notch factor is obtained by treating the pit as a notch at the corroded surface using the notch theory[68] given by

—WILEY—

$$f_n = \frac{1}{k_f} \tag{8}$$

Equation (8) provides the relationship between the notch factor, f_n, and the fatigue stress concentration factor, k_f. The notch factor f_n is greater than 0 and less or equal to 1. The fatigue stress concentration can be defined as the notch sensitivity of the material, q, and the static stress concentration factor, k_{scf}, as given by Equation (9).[69]

$$k_f = 1 + (k_{scf} - 1)q \tag{9}$$

The notch sensitivity, q, is dependent on the diameter of the notch, D[68]:

$$q = \frac{1}{1 + \left(\frac{c}{D}\right)} \tag{10}$$

The static stress concentration, k_{scf}, for a notch with an aspect ratio (a/r or $a/0.5D$) is given by[68]

$$k_{scf} = 1 + 2\sqrt{\frac{a}{0.5D}} \tag{11}$$

After substituting Equations (9)–(11) into Equation (8) and rearranging, the notch factor can be given by

$$f_n = 1 - \frac{2\sqrt{2aD}}{D + c + 2\sqrt{2aD}} \tag{12}$$

The notch sensitivity for steel depends on the UTS.[68] For UTS of 546 MPa (average value for S355 steel reported in the introduction section), the value of the material constant c is 1.05 after fitting to the notch sensitivity data as illustrated in Figure 4.
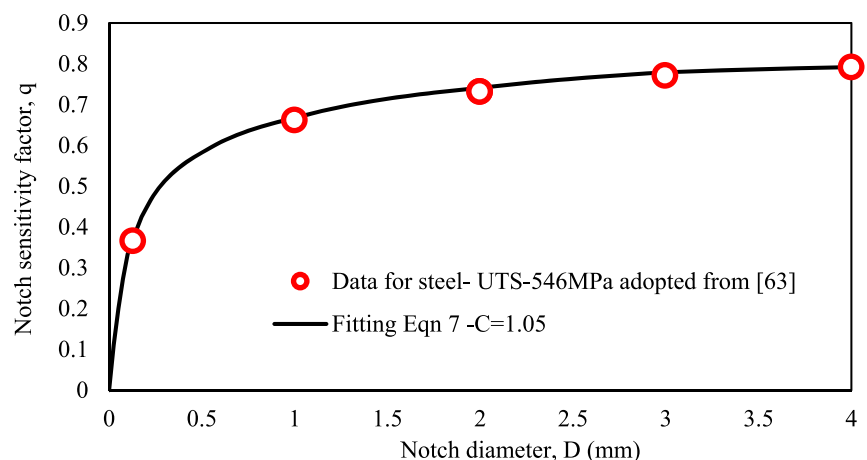
The surface factor, f_s, depends on the UTS and the average surface roughness value, R_a.[58] The validity range for f_s varies with different materials, their surface finish, and the specific roughness measurements (R_a). Values for f_s typically fall in a range between 0.5 and 1, with a value of 1 indicating that the surface roughness does not affect fatigue strength and values less than 1 indicating a reduction in fatigue strength due to the surface finish. The relationship is provided in Figure 5.

Having obtained f_s from Figure 5 and f_n from Equation (12), these values are returned to Equation (7), where f_c can be calculated. Thus, f_c is substituted into Equation (5) to obtain the stress range since the steel material's UTS and R are known. With Equation (6), an S-N curve can be created for every analyzed pit.

3 | RESULTS AND DISCUSSION

Surface deviations for corroded and uncorroded surfaces for two HAZs (HAZ 1 and HAZ 2) were calculated and presented in Figure 6. The surface deviations for HAZ 1 and HAZ 2 locations of the uncorroded specimens were in the range of ±40 μm. However, the corroded specimens showed higher surface deviations in the HAZ zones in the range of ±400 μm. A line separating the weld region and the HAZ region indicated that material loss happened at different weld and base material corrosion rates.

More pits were observable in the HAZ than in the weld regions (Figure 6B,D). The difference suggests higher corrosion resistance at the weld than in the HAZ. It is uncertain whether the welding heat caused microstructural changes that render the HAZ more prone to pitting corrosion. It is, however, an interesting point for future work. Ten critical pits were measured and analyzed for each HAZ. These pits were then characterized by fitting a circular shape at the surface to measure the
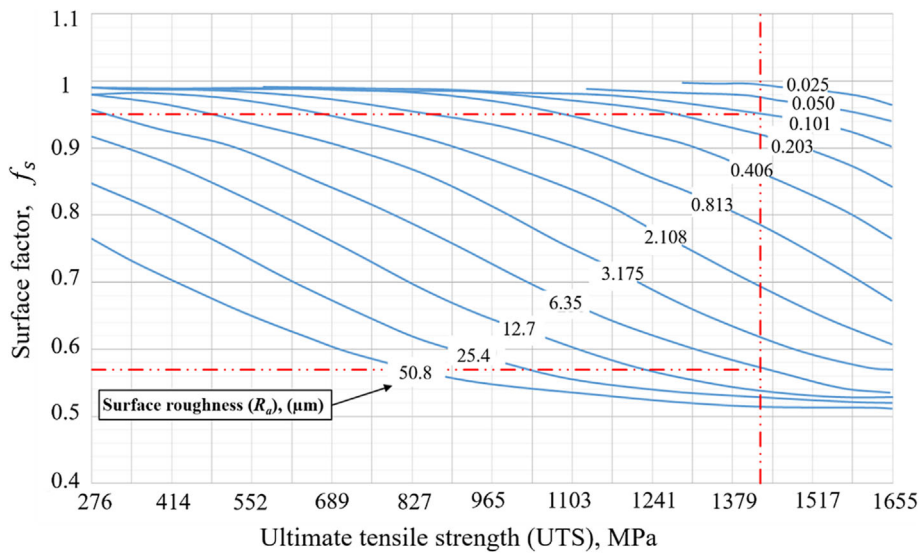

FIGURE 4 Applied notch sensitivity factor for fitting material constant. [Colour figure can be viewed at wileyonlinelibrary.com]

FIGURE 5 Variation of the fatigue surface factor for metal parts plotted against UTS and surface roughness (R_a).[62] [Colour figure can be viewed at wileyonlinelibrary.com]
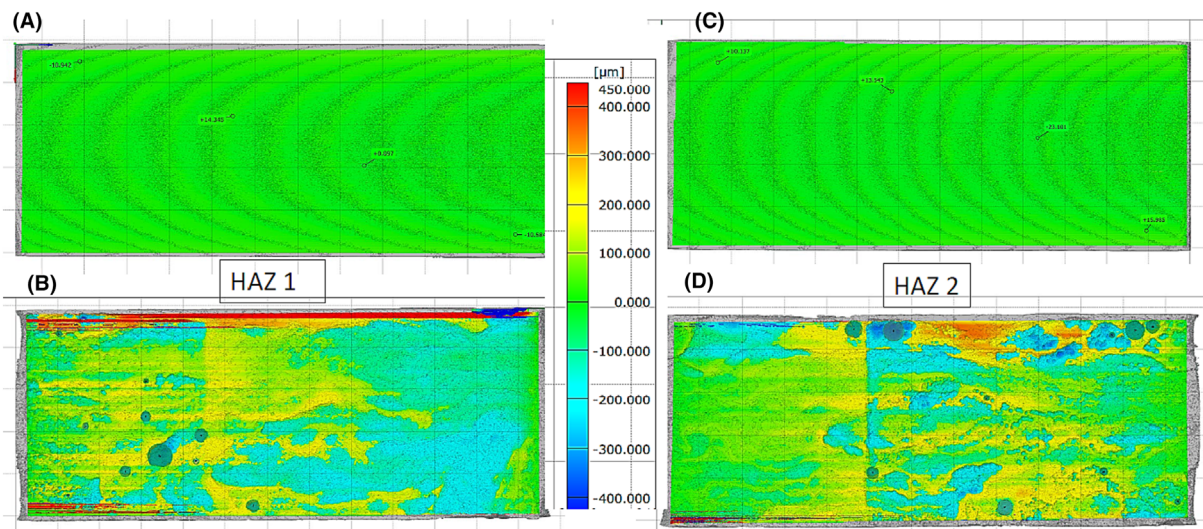

FIGURE 6 Surface deviation plot for (A) uncorroded HAZ 1; (B) corroded HAZ 1; (C) uncorroded HAZ 2; (D) corroded HAZ 2. [Colour figure can be viewed at wileyonlinelibrary.com]

diameters, and the depths of the pits were recorded by obtaining the surface deviation from the top surface of the pit to its center. An example of the measurements is shown in Figure 7.

Surface roughness measurements of the steel surface below the corrosion elements were conducted to assess the surface texture of the corroded sample, as illustrated in Figure 8 from the statistical analysis of the probability distribution associated with the variable depth, which is random. The surface texture was characterized, and the obtained surface properties are provided in Table 1. Since S_a is an area parameter and R_a is a linear parameter, the corrosion surface here is assumed to be completely random (no directional bias), making our surface roughness R_a similar to S_a. R_a of 43.68 μm was obtained and applied

to the corrosion-based fatigue model. Since skewness S_{sk} is $-0.203 < 0$, most measured points were above the mean plane, and the valleys deeper than the peaks were high. This is expected for corrosion as pits are created. The value measured for kurtosis $S_{ku} = 3.648 > 3$, indicated a sharp surface roughness. Observing the skewness and kurtosis values was vital for determining the nature of localized corrosion or corrosion pits. The presence of a negative skewness in the probability density function suggests an occurrence of deep pits on the corroded surface. In statistical terms, this skewness value indicates a distribution with a long tail, which is typical when the corroded surface has deeper, less frequent pits. Also, the kurtosis value demonstrated that the data distribution peaked more due to pit formations. These
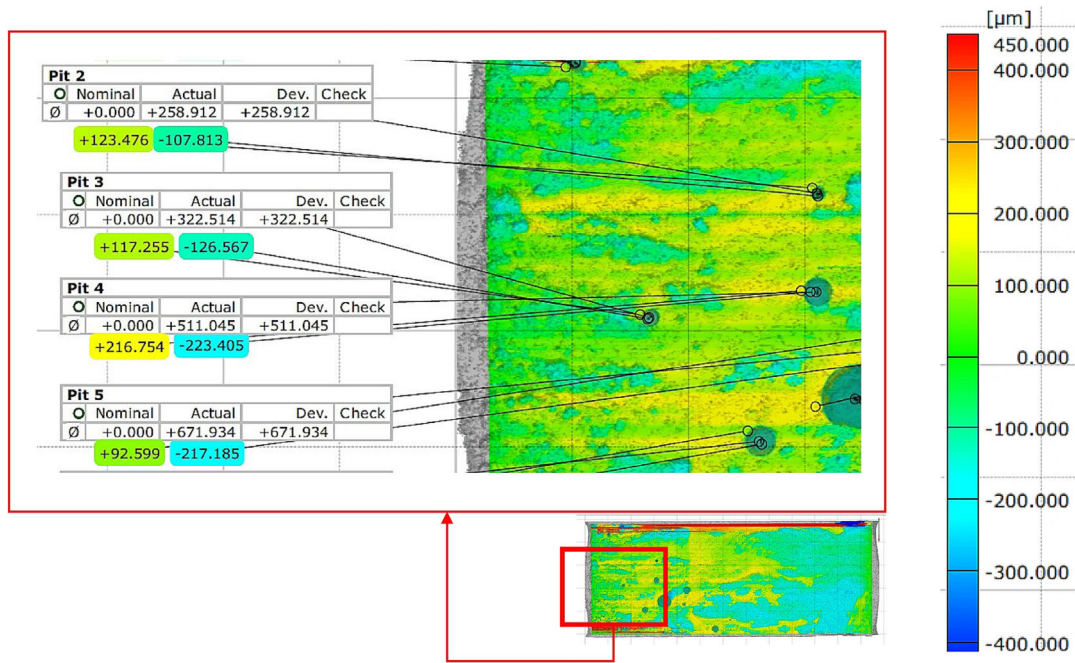
—WILEY—

FIGURE 7 Pit defect parameters obtained on actual pit surface. [Colour figure can be viewed at wileyonlinelibrary.com]
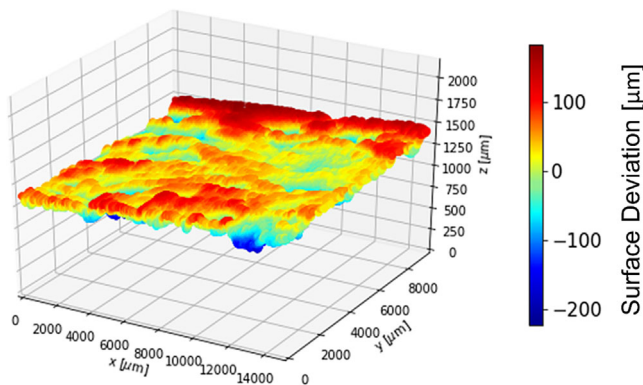

FIGURE 8 Surface texture from a corroded sample (colors represent the distance from a plane that is a fit through all points within the surface). [Colour figure can be viewed at wileyonlinelibrary.com]

TABLE 1 Surface properties for corroded surface according to ISO 25178-2:2021.[66]

Property	Values
Voxel size	12.6338 μm
S_a—arithmetical mean height of the surface compared to the mean plane of the surface $\approx R_a$	43.68 μm
S_q—root mean square height of the surface	57.43 μm
S_{40z}—Average maximum height	402.81 μm
S_{sk}—skewness of the observed surface	−0.203
S_{ku}—measure of the sharpness of the surface roughness	3.648
S_p—highest peak observed within the sampling area	183.83 μm
S_v—deepest valley observed within the same sampling area	−223.84 μm

values agreed with similar results in previous studies where corrosion pits were characterized.[55,56] This is critical information, as the depth and distribution of pits significantly impact the corrosion's structural effect. Thus, the probability density distribution of variable $Z(x, y)$ for the SSC precorroded specimen is presented in Figure 9. For comparability, a R_a value of 16.5 μm has been reported as surface roughness after 80 days in SSC, and if extrapolated to a year, that is extrapolated to 75 μm.[22] This R_a value could be compared to the R_a of 43.68 μm obtained in this study, considering that corrosion changes the surface topology and surface texture over time.

Table 2 presents the characterization of pit properties and their respective fatigue-related factors. The measured pits (diameter and depth) from Figure 6 were selected from both HAZ locations to capture shallow and deep pits. Because the corrosion-based fatigue model predicts a crack to occur from a pit with a circular shape at the surface, the static stress concentration factor at the surface is 3. The pits were classed as shallow pits for an aspect ratio less than one, while the pits were classified as deep for an aspect ratio greater than one. For deep pits, the static stress concentration factor is greater than 3, and the
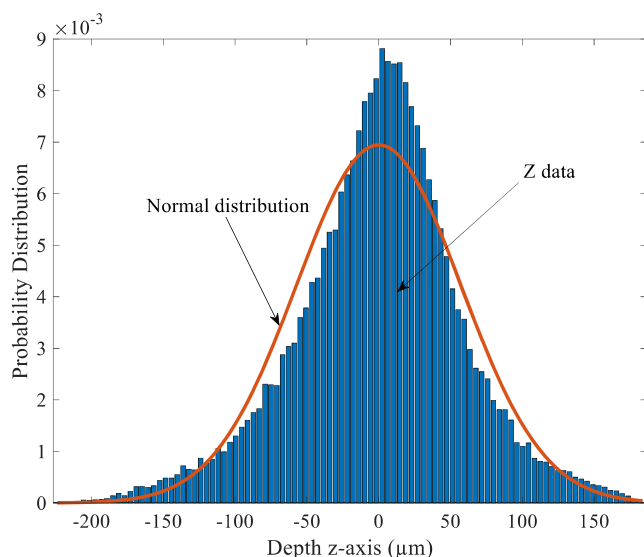
FIGURE 9 Probability density distribution of variable $Z(x, y)$ for precorroded specimen (normal distribution). [Colour figure can be viewed at wileyonlinelibrary.com]

maximum stress is located at the bottom of the pit (view from the surface). For shallow pits, the maximum stress will be at the circular-shaped pit at the surface; hence, the static stress concentration is 3.

The notch sensitivity values were obtained from Figure 4, adapted for S355 structural steel, knowing the pit diameter. The fatigue stress concentration factor k_f values were obtained by substituting the known values of the notch sensitivity factor q and the static stress concentration factor k_{scf} into Equation (9). A surface factor of 0.67 was obtained by relating the measured average surface roughness R_a of 43.68 μm from Table 1 and the UTS of 546 MPa in Figure 5. The notch factor f_n values were obtained by applying the fatigue stress concentration factor k_f into Equation (8). Thus, the corrosion factor f_c values from Equation (7) were obtained as a product of the surface factor of 0.67 and the notch factor.

The corrosion factors for all deep pits ranged from 0.222 to 0.307. The minimum corrosion factor represents the most critical defect, where theoretically the crack should initiate. However, this could be some of the other analyzed critical pits in practice. Therefore, two S-N curves were predicted at $R = 0.5$ with the corrosion-based fatigue model (Section 2.6) using the minimum and the maximum corrosion factors of 0.222 and 0.307, respectively. The two predicted S-N curves were compared with experimental S-N data points obtained at $R = 0.5$ and 0.1.

For clarity, the fatigue tests highlighted in our study are predominantly sourced from the referenced literature to fit the specific corrosion conditions considered in this study. Our experimental approach incorporates surface roughness and CT scanning of specimens into a novel fatigue model developed to elucidate the relationship between pitting corrosion and fatigue. The fatigue testing was performed on S355J2 + N specimens that were butt welded at DTU.[21] These tests took place in a laboratory environment at room temperature, with the specimens subjected to axial tension-tension fatigue testing. The experiments operated at stress ratios of $R = 0.5$ and $R = 0.1$. In the case of specimens tested at $R = 0.5$, any excess weld metal was removed to simulate an ideal condition and to fit the specimens within the testing setup. The welded region of these specimens was fully submerged in an ASW environment maintained at 10°C by a cooling unit throughout the test. The testing was conducted at a frequency of 8 Hz.[21]

For those tested at $R = 0.1$, specimens were kept in their as-welded state. They underwent precorrosion in SSC for 10 days and were then tested in a dry condition. These tests were conducted at a higher frequency of 110 Hz. In all fatigue tests, failure was defined as complete rupture.[22] The derived S-N curves and the results of all axial test series pertaining to mean stress ranges are found in Figure 10. Also, the fatigue strength at 5×10^6 cycles was used for both predicted and experiments. However, the predicted S-N curve followed the design recommendations by the fatigue design code,[51] where the fatigue strength is determined as the value observed at 2×10^6 cycles.

The two predicted mean S-N curves at R of 0.5 and 0.1 (MIN CORROSION FACTOR VALUE) were natural with the data points of the curve D in DNVGL-RP-C203 fatigue code,[51] which was already at mean minus two standard deviations. This was because the background and conditions of the curve from the code (Detail category D4), derived from fatigue tests on butt-welded specimens, and seawater corrosion, aligned with the conditions of the material used in this research for the prediction. The results from the predictions at R of 0.5 and 0.1 (MAX CORROSION FACTOR VALUE) are presented in Figure 10 and validated with fatigue tests in corrosive conditions for corroded S355J2 + N specimens. The results obtained in the high cycle and low-stress range regions verify the influence of the corrosive environment. For $R = 0.5$ at 2×10^6 cycles, the predicted and the tested fatigue strength are 107 MPa and 126 MPa, respectively. For $R = 0.1$ at 2×10^6 cycles, the predicted and tested fatigue strength is 126.3 MPa and 130 MPa, respectively, as illustrated in Figure 11. This direct comparison between predicted and experimental test results indicates that the proposed methodology has great potential in predicting the fatigue strength of corroded structural steel, and it can be applied to the fatigue assessment

TABLE 2 Pit measurements and calculated factors.

Location	Pit no.	Pit diameter, D, mm	Aspect ratio, a/r	Pit type	Static SCF, K_{scf}	Notch sensitivity factor, q	Fatigue SCF, K_f	Notch factor (f_n)	Corrosion factor, f_c (0.67x f_n)
HAZ 1	1	0.838	1.0853	Deep	3.084	0.66	2.375	0.421	0.282
	2	1.001	0.2970	Shallow	3	0.67	1.730	0.578	0.387
	3	0.307	0.7505	Shallow	3	0.515	1.892	0.528	0.354
	4	0.938	0.8656	Shallow	3	0.66	2.228	0.449	0.301
	5	0.659	1.0801	Deep	3.079	0.63	2.309	0.433	0.290
	6	0.291	2.1094	Deep	3.905	0.61	2.772	0.361	0.242
	7	0.612	1.1267	Deep	3.123	0.65	2.380	0.420	0.281
	8	0.792	0.7550	Shallow	3	0.64	2.112	0.473	0.317
	9	0.428	1.4067	Deep	3.372	0.609	2.445	0.409	0.274
	10	0.315	1.2042	Deep	3.195	0.54	2.185	0.458	0.307
HAZ 2	1	0.351	1.4131	Deep	3.378	0.58	2.379	0.420	0.281
	2	0.259	1.7866	Deep	3.673	0.57	2.524	0.396	0.265
	3	0.323	1.5120	Deep	3.459	0.575	2.414	0.414	0.277
	4	0.511	1.7226	Deep	3.625	0.65	2.706	0.370	0.248
	5	0.672	0.9221	Shallow	3	0.62	2.191	0.456	0.306
	6	0.533	0.9765	Shallow	3	0.585	2.156	0.464	0.311
	7	1.207	0.8089	Shallow	3	0.69	2.241	0.446	0.299
	8	0.309	2.1242	Deep	3.915	0.62	2.807	0.356	0.239
	9	0.175	2.9473	Deep	4.434	0.585	3.009	0.332	0.222
	10	0.605	1.1816	Deep	3.174	0.63	2.370	0.422	0.283

FIGURE 10 Predicted and experimental S-N curves and comparison with fatigue codes. [Colour figure can be viewed at wileyonlinelibrary.com]
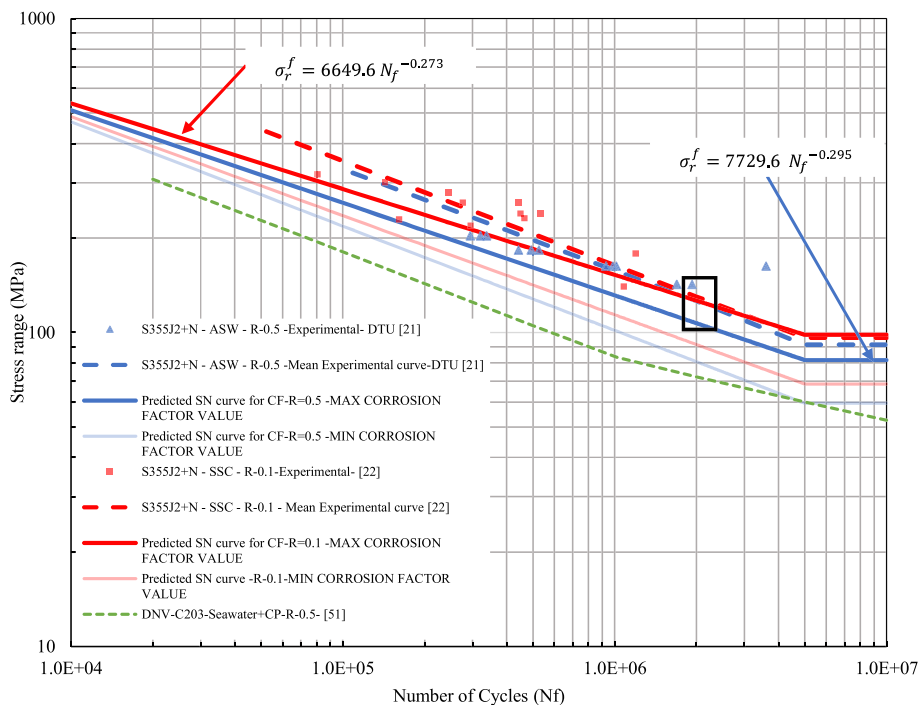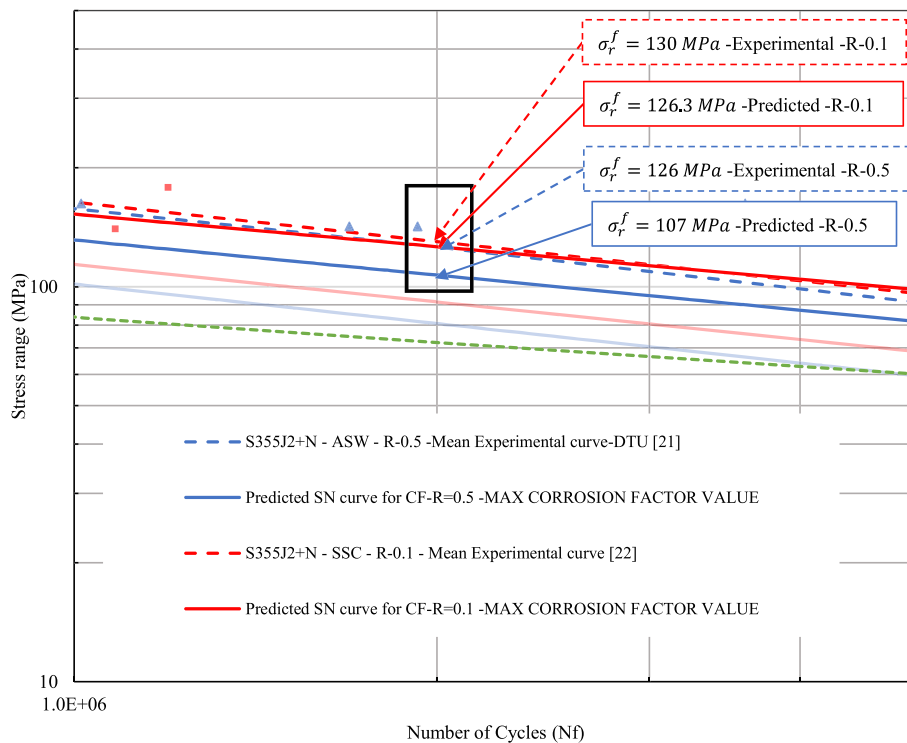
FIGURE 11 Magnified predicted and experimental S-N curves (same scale as Figure 10). [Colour figure can be viewed at wileyonlinelibrary.com]

of welded marine structures. The prediction at $R = 0.1$ was closer than that obtained at $R = 0.5$, possibly because of the slight difference in the type of corrosion environment and the test frequency the specimens were subjected to. Also, this paper demonstrated the capability of the proposed model to consider the mean stress effect, which is important in the fatigue life assessment of marine structures subject to cyclic loads.

This model incorporates pits, stress concentrations, and surface roughness as fatigue crack initiation and propagation sources. However, it does not delve into inherent material properties like residual stresses and the effects of post-welding treatments, which may be seen as a limitation. Also, the CT scans' quality could affect the pit characterization quality. Despite these limitations, the demonstrated predictive performance has shown promise, suggesting these elements could be useful areas for future research and improvements.

4 | CONCLUSIONS

This research paper presented the development of a novel methodology for fatigue assessment of corroded offshore steel welds. The methodology consists of the characterization of a corroded surface and developing a corrosion-based fatigue model capable of predicting S-N curves for critical pits. The following conclusions were derived from this research:

1. The proposed methodology was applied to a welded S355J2 + N steel where a predicted S-N curve at a stress ratio of $R = 0.5$ for a corroded surface was found to be in a close correlation with the fatigue-tested S355J2 + N butt welds.

2. At $R = 0.1$, the predictions closely correlated with experimental findings with a deviation of only 2.8% for similar SSC corrosive conditions. At $R = 0.5$, a deviation of 15.1% was observed.

3. A corroded surface was characterized by critical pits in the heat-affected zones, where deep pits with corrosion factors between 0.222 and 0.307 were identified. The characterization of a corroded surface consisted of measuring a pit diameter, a pit depth, and a surface roughness. The simplicity of the adopted characterization method enables its pragmatic implementation for the inspection of large OWTs in practice.

4. Incorporating corrosion characteristics into the predictive fatigue model can enable the assessment of the remaining life of OWT and other marine structures, which is an important aspect for the future life extension of OWT and their certification.

5. The fatigue model's capability to consider the mean stress effect gives the advantage of conducting more realistic fatigue assessments for a transient in nature stress field induced by cyclic wind and wave loads.

6. In future work, the proposed methodology is aimed to be applied to assess the remaining life of an offshore

asset (e.g., OWT), where the remaining life can be determined by the history of the loads and the corrosion topology of the surface.

NOMENCLATURE

KeV	energy
D	diameter
r	radius
a	pit depth
σ_a^f	stress amplitude
σ_r^f	stress range
σ_m	mean stress
c	material constant
f_c	corrosion factor
f_n	notch factor
f_s	surface factor
q	notch sensitivity

AUTHOR CONTRIBUTIONS

Victor Okenyi: Writing; conceptualization; methodology; software. **Shukri Afazov**: Reviewing; editing; theory; supervision. **Neil Mansfield**: Supervision. **Martin Alexander Eder**: Reviewing; editing. **Asger Bech Abrahamsen**: Reviewing; materials. **Søren Fæster**: Reviewing; editing; software. **Christopher Gottlieb Klingaad**: Reviewing; computer programming. **Petros Siegkas**: Reviewing; supervision. **Mahdi Bodaghi**: Analysis; reviewing; editing; supervision.

ACKNOWLEDGMENTS

DATA AVAILABILITY STATEMENT

Data sharing is not applicable to this article as no new data were created or analyzed in this study.

ORCID

Victor Okenyi https://orcid.org/0000-0001-6489-2675

REFERENCES

1. Sun X, Huang D, Wu G. The current state of offshore wind energy technology development. *Energy*. 2012;41(1):298-312.
2. Hutchinson M, Zhao F. Global Wind Report 2023. Brussels; 2023.
3. Velarde J, Bachynski EE. Design and fatigue analysis of monopile foundations to support the DTU 10 MW offshore wind turbine. *Energy Procedia*. 2017;137:3-13.
4. Okenyi V, Bodaghi M, Mansfield N, Afazov S, Siegkas P. A review of challenges and framework development for corrosion fatigue life assessment of monopile-supported horizontal-axis offshore wind turbines. *Ships Offshore Struct*. 2022;1-15.
5. Igwemezie V, Mehmanparast A, Kolios A. Materials selection for XL wind turbine support structures: a corrosion-fatigue perspective. *Mar Struct*. 2018;61:381-397.
6. Biswal R, Al Mamun A, Mehmanparast A. On the performance of monopile weldments under service loading conditions and fatigue damage prediction. *Fatigue Fract Eng Mater Struct*. 2021;44(6):1469-1483.
7. Hoeppner D. Model for prediction of fatigue lives based upon a pitting corrosion fatigue process. In: *Fatigue Mechanisms*. ASTM International; 1979:841-870.
8. Liao D, Zhu SP, Correia JAFO, de Jesus AMP, Berto F. Recent advances on notch effects in metal fatigue: a review. *Fatigue Fract Eng Mater Struct*. 2020;43(4):637-659.
9. Kolios A, Wang L, Mehmanparast A, Brennan F. Determination of stress concentration factors in offshore wind welded structures through a hybrid experimental and numerical approach. *Ocean Eng*. 2019;178:38-47.
10. Milone A, Landolfo R, Berto F. Methodologies for the fatigue assessment of corroded wire ropes: a state-of-the-art review. *Structure*. 2022;37:787-794.
11. Balbín JA, Chaves V, Larrosa NO. Pit to crack transition and corrosion fatigue lifetime reduction estimations by means of a short crack microstructural model. *Corros Sci*. 2021;180:109171.
12. Mehmanparast A, Brennan F, Tavares I. Fatigue crack growth rates for offshore wind monopile weldments in air and seawater: SLIC inter-laboratory test results. *Mat Des*. 2017;114: 494-504.
13. Remes H, Gallo P, Jelovica J, Romanoff J, Lehto P. Fatigue strength modelling of high-performing welded joints. *Int J Fatigue*. 2020;135:105555.
14. Farhad F, Smyth-Boyle D, Zhang X. Fatigue of X65 steel in the sour corrosive environment—a novel experimentation and analysis method for predicting fatigue crack initiation life from corrosion pits. *Fatigue Fract Eng Mater Struct*. 2021;44(5):1195-1208.
15. Adasooriya ND, Pavlou D, Hemmingsen T. Fatigue strength degradation of corroded structural details: a formula for S-N curve. *Fatigue Fract Eng Mater Struct*. 2020;43(4): 721-733.
16. Ryan H, Mehmanparast A. Development of a new approach for corrosion-fatigue analysis of offshore steel structures. *Mech Mater*. 2023;176:104526.
17. Larrosa NO, Akid R, Ainsworth RA. Corrosion-fatigue: a review of damage tolerance models. *Int Mater Rev*. 2018;63(5): 283-308.
18. Sonsino CM. Effect of residual stresses on the fatigue behaviour of welded joints depending on loading conditions and weld geometry. *Int J Fatigue*. 2009;31(1):88-101.
19. Ohta A, Suzuki N, Maeda Y. Shift of S-N curves with stress ratio. *Welding in the World*. 2003;47(1-2):19-24.
20. Pedersen MM. Thickness effect in fatigue of welded butt joints: a review of experimental works. *Int J Steel Struct*. 2019;19(6): 1930-1938.
21. Ólafsson ÓM, Berggreen C. *Improved Design Basis of Welded Joints in Seawater*. DTU Mechanical Engineering; 2016.
22. Gkatzogiannis S, Weinert J, Engelhardt I, Knoedel P, Ummenhofer T. Correlation of laboratory and real marine corrosion for the investigation of corrosion fatigue behaviour of steel components. *Int J Fatigue*. 2019;126:90-102.

23. Gkatzogiannis S, Weinert J, Engelhardt I, Knoedel P, Ummenhofer T. Corrosion fatigue behaviour of HFMI-treated butt welds. *Int J Fatigue*. 2021;145:106079.

24. Daavari M, Sadough Vanini SA. Corrosion fatigue enhancement of welded steel pipes by ultrasonic impact treatment. *Mater Lett*. 2015;139:462-466.

25. Fereidooni B, Morovvati MR, Sadough-Vanini SA. Influence of severe plastic deformation on fatigue life applied by ultrasonic peening in welded pipe 316 stainless steel joints in corrosive environment. *Ultrasonics*. 2018;88:137-147.

26. Knysh V v, Solovei SA, Kir'yan VI, Bulash VN. Increasing the corrosion fatigue resistance of welded joints by high-frequency mechanical peening. *Strength Mater*. 2018;50(3):443-447.

27. Klusák J, Seitl S. Very high cycle fatigue tests of high strength steels S355 J0 and S355 J2. *Procedia Struct Integr*. 2019;17:576-581.

28. Weich I, Ummenhofer T, Nitschke-Pagel T, Dilger K, Eslami CH. Fatigue behaviour of welded high-strength steels after high frequency mechanical post-weld treatments. *Weld World*. 2009;53(11-12):R322-R332.

29. Madia M, Zerbst U, Th. Beier H, Schork B. The IBESS model—elements, realisation and validation. *Eng Fract Mech*. 2018;198:171-208.

30. Nazzal SS, Mikkola E, Yıldırım HC. Fatigue damage of welded high-strength steel details improved by post-weld treatment subjected to critical cyclic loading conditions. *Eng Struct*. 2021;237:111928.

31. Wang T, Wang D, Huo L, Zhang Y. Discussion on fatigue design of welded joints enhanced by ultrasonic peening treatment (UPT). *Int J Fatigue*. 2009;31(4):644-650.

32. Saidin S, Andud D, Manurung YHP, MuhdF M, Nordin N, Leitner M. Effects of high frequency mechanical impact on fatigue life of semi-automated gas metal arc welding (GTAW) of HSLA butt weld. *MATEC Web of Conferences*. 2019;269:06002.

33. Ummenhofer T, Weidner P. Improvement factors for the design of welded joints subjected to high frequency mechanical impact treatment. *Steel Constr*. 2013;6(3):191-199.

34. Weich I. *Ermüdungsverhalten mechanisch nachbehandelter Schweißverbindungen in Abhängigkeit des Randschichtzustands*. Institut für Bauwerkserhaltung und Tragwerk; 2009.

35. Corigliano P, Epasto G, Guglielmino E, Risitano G. Fatigue analysis of marine welded joints by means of DIC and IR images during static and fatigue tests. *Eng Fract Mech*. 2017;183:26-38.

36. Corigliano P, Cucinotta F, Guglielmino E, Risitano G, Santonocito D. Fatigue assessment of a marine structural steel and comparison with thermographic method and static thermographic method. *Fatigue Fract Eng Mater Struct*. 2020;43(4):734-743.

37. Tong L, Niu L, Ren Z, Zhao XL. Experimental investigation on fatigue behavior of butt-welded high-strength steel plates. *Thin-Walled Struct*. 2021;165:107956.

38. Leitner M, Stoschka M, Eichlseder W. Fatigue enhancement of thin-walled, high-strength steel joints by high-frequency mechanical impact treatment. *Weld World*. 2014;58(1):29-39.

39. Schiller R, Oswald M, Neuhäusler J, Rother K, Engelhardt I. Fatigue strength of partial penetration butt welds of mild steel. *Weld World*. 2022;66(12):2563-2584.

40. Schaumann P, Vermeulen M, Keindorf C, et al. High Frequency Fatigue Testing of Butt Welds with a New Magnet Resonance Machine Structural Fire Design View Project Probabilistische Sicherheitsbewertung von Offshore-Windenergieanlagen View Project High Frequency Fatigue Testing of Butt Welds with a New Magnet Resonance Machine.2010.

41. Čern I, Sís J. Evaluation of fatigue strength of different thickness laser welded s355 steel sheets considering microstructure, surface conditions and residual stresses. In: *Key Engineering Materials*. Vol. 713. Trans Tech Publications Ltd; 2016:82-85.

42. Sorger G, Lehtimäki E, Hurme S, Remes H, Vilaça P, Molter L. Microstructure and fatigue properties of friction stir welded high-strength steel plates. *Sci Technol Weld Join*. 2018;23(5):380-386.

43. Köder T, Bohlmann B. Experimental fatigue analysis of butt-welded joints. *Ship Technol Res*. 2014;61(3):132-141.

44. Schaumann P, Steppeler S. Fatigue tests of axially loaded butt welds up to very high cycles. *Procedia Eng*. 2013;66:88-97.

45. Braun M. Statistical analysis of sub-zero temperature effects on fatigue strength of welded joints. *Weld World*. 2022;66(1):159-172.

46. Anandavijayan S, Mehmanparast A, Braithwaite J, Brennan F, Chahardehi A. Material pre-straining effects on fatigue behaviour of S355 structural steel. *J Constr Steel Res*. 2021;183:106707.

47. Mehmanparast A, Taylor J, Brennan F, Tavares I. Experimental investigation of mechanical and fracture properties of offshore wind monopile weldments: SLIC interlaboratory test results. *Fatigue Fract Eng Mater Struct*. 2018;41(12):2485-2501.

48. Jacob A, Mehmanparast A, D'Urzo R, Kelleher J. Experimental and numerical investigation of residual stress effects on fatigue crack growth behaviour of S355 steel weldments. *Int J Fatigue*. 2019;128:105196.

49. Yusof F, Jamaluddin MF. Welding defects and implications on welded assemblies. In: *Comprehensive Materials Processing*. Vol. 6. Elsevier Ltd; 2014:125-134.

50. BS 7608:2014. Guide to Fatigue Design and Assessment of Steel Products (+A1:2015). London; 2014.

51. DNV G. Fatigue design of offshore steel structures. Recommended Practice DNVGL-RP-C203. 2016;20: 2016.

52. BS EN 1993-1-9:2005 Eurocode 3: Design of Steel Structures. Fatigue. London; 2005.

53. International Institute of Welding (IIW). Recommendations For Fatigue Design of Welded Joints And Components. Paris; 2008.

54. Jacob A, Mehmanparast A. Crack growth direction effects on corrosion-fatigue behaviour of offshore wind turbine steel weldments. *Mar Struct*. 2021;75:102881.

55. To D, Umezawa O, Shinohara T. Detection of surface roughness evolution of carbon steel subjected to outdoor exposure and constant humidity corrosion tests. In: *Materials Transactions*. Vol. 59. Japan Institute of Metals (JIM); 2018:1239-1243.

56. Nugroho FA, Braun M, Ehlers S. Probability analysis of PIT distribution on corroded ballast tank. *Ocean Eng*. 2021;228:108958.

57. Nugroho FA, Garhuom W, Andresen-Paulsen G, Ehlers S. Numerical analysis of the correlation between the pitting

severity and surface roughness of corroded specimens. *Ships Offshore Struct*. 2022;17(12):2699-2714.

58. Serjouei A, Afazov S. Predictive model to design for high cycle fatigue of stainless steels produced by metal additive manufacturing. *Heliyon*. 2022;8(11):e11473.

59. Veritas DN. DNVGL-RP-0416: Corrosion Protection for Wind Turbines. 2016.

60. Feldkamp LA, Davis LC, Kress JW. Practical cone-beam algorithm. *J Opt Soc Am A*. 1984;1(6):612-619.

61. Thermo Fisher Scientific. Thermo Scientific TM Avizo TM Software 9 User's Guide. 1995.

62. ZEISS Group. GOM Inspect Software Evaluation Software for 3D Point Clouds. 2021.

63. Python Software Foundation. Python Language Reference, version 3.11. 2022.

64. Klingaa CG, Bjerre MK, Baier S, de Chiffre L, Mohanty S, Hattel JH. Roughness investigation of SLM manufactured conformal cooling channels using X-ray computed tomography. In: Proceedings of the 9th Conference on Industrial Computed Tomography (ICT 2019), Padova, Italy; 2019:13-15, 3.

65. Ferreira T, Rasband W. ImageJ User Guide ImageJ User Guide IJ Version 1.51w. 2018.

66. ISO 25178-2:2021 Geometrical Product Specifications (GPS) — Surface Texture: Areal — Part 2: Terms, Definitions and Surface Texture Parameters. Geneva; 2021.

67. Bannantine JA, Comer JJ, Handrock JL. Fundamentals of metal fatigue analysis. 1990.

68. Peterson R. Relation between life testing and conventional tests of materials. Bulletin ASTM. 1945.

69. Sines G, Waisman JL, Dolan TJ. *Metal Fatigue*. McGraw-Hill; 1959.